ISSN 1674-1056
http://cpb.iphy.ac.cn
http://iopscience.iop.org/cpb
中国物理 B
Chinese Physics
中国物理
Chinese Physics B

The nonlocal transport and switch effect in light- and electric-controlled silicene-superconductor hybrid structure

Fenghua Qi(戚凤华), Jun Cao(曹军), Jie Cao(曹杰), Lifa Zhang(张力发)

Citation: Chin. Phys. B . 2018, 27(12): 127401. **doi:** 10.1088/1674-1056/27/12/127401

What follows is a list of articles you may be interested in

Transition from tunneling regime to local point contact realized on $Ba_{0.6}K_{0.4}Fe_2As_2$ surface

Xingyuan Hou(侯兴元), Yunyin Jie(揭云印), Jing Gong(巩靖), Bing Shen(沈冰), Hai Zi(子海), Chunhong Li(李春红), Cong Ren(任聪), Lei Shan(单磊)

Chin. Phys. B . 2017, 26(6): 067402. **doi:** 10.1088/1674-1056/26/6/067402

Spatially resolved gap closing in single Josephson junctions constructed on Bi_2Te_3 surface

Yuan Pang(庞远), Junhua Wang(王骏华), Zhaozheng Lyu(吕昭征), Guang Yang(杨光), Jie Fan(樊洁), Guangtong Liu(刘广同), Zhongqing Ji(姬忠庆), Xiunian Jing(景秀年), Changli Yang(杨昌黎), Li Lu(吕力)

Chin. Phys. B . 2016, 25(11): 117402. **doi:** 10.1088/1674-1056/25/11/117402

Electronic structure of silicene

L. C. Lew Yan Voon

Chin. Phys. B . 2015, 24(8): 087309. **doi:** 10.1088/1674-1056/24/8/087309

Silicene on substrates: A theoretical perspective

Zhong Hong-Xia, Quhe Ru-Ge, Wang Yang-Yang, Shi Jun-Jie, Lü Jin

Chin. Phys. B . 2015, 24(8): 087308. **doi:** 10.1088/1674-1056/24/8/087308

Josephson current versus potential strength of the interface in ferromagnetic superconductors

Hamidreza Emamipour

Chin. Phys. B . 2014, 23(5): 057402. **doi:** 10.1088/1674-1056/23/5/057402

SPECIAL TOPIC — 60th Anniversary of Department of Physics of Nanjing Normal University

The nonlocal transport and switch effect in light- and electric-controlled silicene–superconductor hybrid structure*

Fenghua Qi(戚凤华)[1,2], Jun Cao(曹军)[1,2], Jie Cao(曹杰)[3], and Lifa Zhang(张力发)[1,†]

[1] Center for Quantum Transport and Thermal Energy Science, School of Physics and Technology, Nanjing Normal University, Nanjing 210023, China
[2] School of Electronic Engineering, Nanjing Xiaozhuang University, Nanjing 211171, China
[3] College of Science, Hohai University, Nanjing 210098, China

(Received 22 August 2018; revised manuscript received 2 November 2018; published online 25 November 2018)

We theoretically investigate the influence of off-resonant circularly polarized light field and perpendicular electric field on the quantum transport in a monolayer silicene-based normal/superconducting/normal junction. Owing to the tunable band structure of silicene, a pure crossed Andreev reflection process can be realized under the optical and electrical coaction. Moreover, a switch effect among the exclusive crossed Andreev reflection, the exclusive elastic cotunneling and the exclusive Andreev reflection, where the former two are the nonlocal transports and the third one is the local transport, can be obtained in our system by the modulation of the electric and light fields. In addition, the influence of the relevant parameters on the nonlocal and local transports is calculated and analyzed as well.

Keywords: switch effect, silicene, crossed Andreev reflection

PACS: 74.45.+c, 73.23.Ad, 85.25.–j **DOI:** 10.1088/1674-1056/27/12/127401

1. Introduction

As the silicon counterpart of graphene, silicene has attracted much attention in quantum condensed matter research.[1,2] Owing to the low buckling structure, the energy gap of silicene can be controlled by applying electric field to create staggered potential.[3–7] Moreover, silicene possesses a strong spin-orbit coupling which is much larger than that in graphene, making it to be a quantum spin Hall insulator in nature.[8,9] Experimentally, many researchers have successfully synthesized silicene on kinds of substrates such as Ag(111), ZrB_2(0001), Ir(111), and MoS_2.[10–15] These unique properties make silicene a promising candidate for logic application.[16] In addition, there have already been some studies about proximity-induced superconductivity in silicene, which open up a research area involving coherent transport properties in silicene-based superconducting hybrid structures.[17–23]

Recently, the entanglement of quantum states has aroused great interests for its potential applications and fundamental importance in quantum information technology.[24–27] In solid state physics, it still remains a major challenge to create and detect entangled electrons. S-wave superconductors have been viewed as natural sources for entangled electrons, since a singlet Cooper pairs consist of two electrons with both spin and momentum entangled.[28,29] The crossed (nonlocal) Andreev refection (CAR) in superconducting heterostructures refers to that an electron from a normal metal electrode is incident into the superconducting region and reflected as a hole in another metal electrode.[30–32] Therefore the inverse process of the CAR is proposed to be a natural method to split a Cooper pair spatially.[33–35]

However, there also exist other accompanied processes such as the (local) Andreev reflection (AR), where the hole is reflected into the same terminal, the elastic cotunneling (EC, another nonlocal process), and the normal reflection (NR). These transport processes can mask the CAR and make its detection difficult in experiments.[36–38] Hence a lot of proposals have been put forward to increase the fraction of the CAR.[17,18,39–46] A graphene bipolar transistor is proposed to generate the pure CAR using energy band topology or the energy-filtering mechanism.[39,40] Some superconducting spin valve structures based on graphene, silicene and MoS_2 are designed to obtain the pure CAR process.[18,41,42] In addition, it has been demonstrated that the fraction of the CAR can be enhanced a lot in the hybrid systems of the superconductor and the topological insulators.[43–45]

In this paper, we consider the quantum transport in a silicene-based normal/superconducting/normal (N/S/N) junction with the applied off-resonant circularly polarized light field and perpendicular electric field. By the optical and electrical modulation of the bands in the two normal regions, the exclusive CAR can be achieved with the suppression of the AR and the EC processes. Moreover, the exclusive EC and AR transports can also be obtained respectively by setting the

*Project supported by the National Natural Science Foundation of China (Grant Nos. 11504084 and 11647164) and the Natural Science Foundation for Colleges and Universities in Jiangsu Province, China (Grant Nos. 18KJB140005, 17KJD170004, and 16KJB140008).

†Corresponding author. E-mail: phyzlf@njnu.edu.cn

© 2018 Chinese Physical Society and IOP Publishing Ltd

proper parameters. It means that our system can realize a switch effect among the exclusive CAR, EC, and AR. These results reveal the potential of silicene-based hybrid structures for application in the correlation transport.

We organize this work as follows. In Section 2, we establish the theoretical framework which will be used to calculate the local and nonlocal conductances. In Section 3, we present the numerical results. Finally, we give a brief summary of the results in Section 4.

2. Model and formalism

We consider an N/S/N junction based on monolayer silicene, as illustrated in Fig. 1(a), where N represents two normal regions and S represents proximity-induced superconductiviting region. An off-resonant circularly polarized light, which just modifies the electron band structure through virtual photon transition processes,[47,48] and a perpendicular electric field are applied onto the two normal regions. The x–y coordinates are used to characterize the longitudinal and transverse directions in our system. For studying the possible transport properties through the system, we begin with the tight-binding Hamiltonian of this system expressed as[9]

$$H_{\mathrm{T}} = H_{\mathrm{S}} + H_{\mathrm{N}}. \tag{1}$$

Therein, H_{S} and H_{N} are respectively the Hamiltonians of the superconducting region and the two normal regions. They have the following forms:

$$\begin{aligned} H_{\mathrm{S}} &= H_0 + \sum_m \Delta (c^{\dagger}_{m\uparrow} c^{\dagger}_{m\downarrow} + c_{m\downarrow} c_{m\uparrow}) \\ &\quad + \sum_{m\alpha} U_{\mathrm{S}} c^{\dagger}_{m\alpha} c_{m\alpha}, \end{aligned} \tag{2}$$

$$\begin{aligned} H_{\mathrm{N}} &= H_0 - \frac{\mathrm{i}\lambda}{3\sqrt{3}} \sum_{\langle\langle m,n\rangle\rangle,\alpha,\beta} \nu_{mn} c^{\dagger}_{m\alpha} c_{n\beta} \\ &\quad + \sum_{m,\alpha,\kappa} \mu_m e l E_z^{\kappa} c^{\dagger}_{m,\alpha,\kappa} c_{m,\alpha,\kappa} \\ &\quad + \sum_{m,\alpha,\kappa} U_{\kappa} c^{\dagger}_{m,\alpha,\kappa} c_{m,\alpha,\kappa}, \end{aligned} \tag{3}$$

where the zero external-field Hamiltonian is[49]

$$\begin{aligned} H_0 &= -t_0 \sum_{\langle m,n\rangle,\alpha} c^{\dagger}_{m\alpha} c_{n\alpha} \\ &\quad + \frac{\mathrm{i}\lambda_{\mathrm{SO}}}{3\sqrt{3}} \sum_{\langle\langle m,n\rangle\rangle,\alpha,\beta} \nu_{mn} c^{\dagger}_{m\alpha} \sigma^z_{\alpha\beta} c_{n\beta}. \end{aligned} \tag{4}$$

In Eqs. (2)–(4), $c_{m\alpha}$ ($c^{\dagger}_{m\alpha}$) annihilates (creates) an electron with spin α on site m, U_{S} is the chemical potential of the superconducting region, which is set as 0.03 eV in the following, Δ is the pairing potential and $\lambda = (eAv_{\mathrm{F}})^2/\hbar\Omega$ is the illumination parameter with A as the amplitude and Ω as the frequency of the off-resonant right-circularly polarized light, as defined in the Floquet theory. In addition, to satisfy the off-resonant condition, the photon energy $\hbar\Omega$ must be larger than the silicene bandwidth $3t_0$, where $t_0 = 1.6$ eV is the nearest-neighbor hopping energy. Hence, the lowest value of Ω is about 1150 THz. An applied perpendicular electric field E_z^{κ} can generate a staggered sublattice potential $el\mu_m E_z^{\kappa}$ in region κ ($\kappa = \mathrm{L}$ for the left region and $\kappa = \mathrm{R}$ for the right region), where e is the electron charge, $2l = 0.46$ Å is the separation between the A and B sublattices in the z direction, as denoted in Fig. 1(b), and $\mu_m = \pm 1$ for the A (B) sites. U_{κ} is the chemical potential of the two normal regions. $\lambda_{\mathrm{SO}} = 3.9$ meV is the effective spin-orbit coupling parameter and $\boldsymbol{\sigma} = (\sigma_x, \sigma_y, \sigma_z)$ is the Pauli matrix of spin. $\langle m,n\rangle$ and $\langle\langle m,n\rangle\rangle$ denote the summations over the nearest and next-nearest neighboring lattice sites, respectively. $\nu_{mn} = -1$ when the next-nearest neighbor hopping is clockwise and $\nu_{mn} = 1$ when the hopping is anticlockwise with respect to the normal regions of the monolayer silicene sheet.

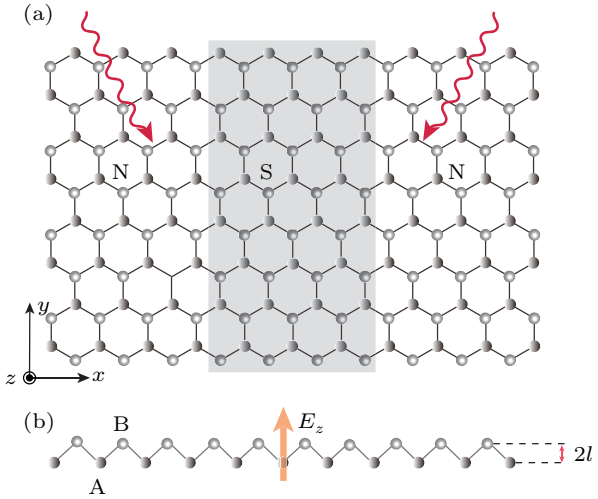


Fig. 1. (color online) Schematics for (a) the top view of a monolayer silicene-based N/S/N junction with two normal regions irradiated by the off-resonant circularly polarized light and applied with the perpendicular electric field and (b) the side view of silicene applied with the perpendicular electric field. Two inequivalent atoms are labeled as A and B. $2l$ represents the distance between the A and B sublattices in the z direction.

Band structure of a system can be effectively used to account for its transport properties. For conveniently obtaining the band structure of the left or right normal region, we need to transform Eq. (3) into the momentum space form as given below[9]

$$\begin{aligned} H_{\eta}^{\kappa} &= \hbar v_{\mathrm{F}} (\eta k_x \tau_x + k_y \tau_y) + \eta \lambda_{\mathrm{SO}} s \tau_z \\ &\quad - e l E_z^{\kappa} \tau_z - \eta \lambda \tau_z - U_{\kappa} \boldsymbol{I}, \end{aligned} \tag{5}$$

where $\eta = 1$ (-1) for K (K′) valley, $v_{\mathrm{F}} = 3at_0/2\hbar$ is the Fermi velocity with the lattice constant $a = 3.86$ Å, k_x and k_y are the wavevectors in the x and y directions, $\boldsymbol{\tau} = (\tau_x, \tau_y, \tau_z)$ is the Pauli matrix of sublattice pseudospin, $s = \pm 1$ is the spin index and $\boldsymbol{I}$ is the identity matrix.

Combining the three kinds of main transports, the total conductance can be written as[46]

$$\begin{aligned} g &= g_{\rm EC} + g_{\rm AR} + g_{\rm CAR} \\ &= \frac{e}{hW}\sum_{k_y} {\rm Tr}\{\Gamma_{\rm Lee} G^{\rm r}_{\rm ee} \Gamma_{\rm Ree} G^{\rm a}_{\rm ee} + 2\Gamma_{\rm Lee} G^{\rm r}_{\rm eh} \Gamma_{\rm Lhh} G^{\rm a}_{\rm he} \\ &\quad + \Gamma_{\rm Lee} G^{\rm r}_{\rm eh} \Gamma_{\rm Rhh} G^{\rm a}_{\rm he}\}, \end{aligned} \tag{6}$$

where $g_{\rm EC}$, $g_{\rm AR}$, and $g_{\rm CAR}$ respectively represent the conductance of the EC, the local AR, and the nonlocal CAR. $k_y = 2\pi n/W$ is the transverse momentum with n being an integer to denote the channels and W representing the transverse width of the junction. The linewidth function $\Gamma_{\rm L(R)}$ can be defined as $\Gamma_{\rm L(R)} = {\rm i}(\Sigma^{\rm r}_{\rm L(R)} - \Sigma^{\rm a}_{\rm L(R)})$, where $\Sigma^{\rm r(a)}_{\rm L(R)} = V^{\dagger} g^{\rm r(a)}_{\rm L(R)} V$ is the self-energy of the left (right) region. V is the coupling matrix between the leads and the central region. $g^{\rm r(a)}_{\rm L(R)}$ is the retarded (advanced) surface Green's function of the left (right) region, which can be calculated by a recursive iteration method.[50,51] $G^{\rm r(a)} = (E{\rm I} - H_{\rm S} - \Sigma^{\rm r(a)})^{-1}$ stands for the retarded (advanced) Green's function of the central region, where $\Sigma^{\rm r(a)} = \Sigma^{\rm r(a)}_{\rm L} + \Sigma^{\rm r(a)}_{\rm R}$. The subscript e (h) denotes the electron (hole) component of the Nambu space.

3. Results and discussion

3.1. Pure crossed Andreev reflection

In Ref. [43], we have discussed the nonlocal transport in the bilayer graphene just induced by the valley polarization, where the spin degree of freedom is degenerate and inactive, and is not be involved in our investigation. Different from the bilayer graphene system, there exists the spin–orbit coupling in the silicene. The degeneration of the spin and valley degrees of freedom can be lifted at the same time under the coaction of the off-resonant circularly polarized light and the perpendicular electric field. Hence, in the following discussion, we must consider the effect of the spin degree of freedom. In order to reveal the non-degeneracy of the band structure more clearly, we first analytically give the energy eigenvalues of different spins and valleys in the two normal regions:

$$\varepsilon^{\kappa}_{\eta\sigma} = \pm\sqrt{(\hbar v_{\rm F} k)^2 + (\eta\sigma\lambda_{\rm SO} - elE^{\kappa}_z - \eta\lambda)^2}. \tag{7}$$

Correspondingly, on the K and K′ points, equation (7) can be simplified into the following forms:

$$\begin{aligned} \varepsilon^{\kappa}_{{\rm K}\uparrow} &= \pm(\lambda_{\rm SO} - elE^{\kappa}_z - \lambda), \\ \varepsilon^{\kappa}_{{\rm K}\downarrow} &= \pm(\lambda_{\rm SO} + elE^{\kappa}_z + \lambda), \\ \varepsilon^{\kappa}_{{\rm K}'\uparrow} &= \pm(\lambda_{\rm SO} + elE^{\kappa}_z - \lambda), \\ \varepsilon^{\kappa}_{{\rm K}'\downarrow} &= \pm(\lambda_{\rm SO} - elE^{\kappa}_z + \lambda). \end{aligned} \tag{8}$$

Obviously, the degeneration of the spin and valley can be controlled by the electric field and the light field.

In Fig. 2, we set $\lambda = 3\lambda_{\rm SO}$ and $elE^{\rm L}_z = -elE^{\rm R}_z = \lambda$, so equation (8) can be further simplified as: $\varepsilon^{\rm L}_{{\rm K}\uparrow} = \pm 5\lambda_{\rm SO}$, $\varepsilon^{\rm L}_{{\rm K}\downarrow} = \pm 7\lambda_{\rm SO}$, $\varepsilon^{\rm L}_{{\rm K}'\uparrow} = \varepsilon^{\rm L}_{{\rm K}'\downarrow} = \pm\lambda_{\rm SO}$ for the left region and $\varepsilon^{\rm R}_{{\rm K}\uparrow} = \varepsilon^{\rm R}_{{\rm K}\downarrow} = \pm\lambda_{\rm SO}$, $\varepsilon^{\rm R}_{{\rm K}'\uparrow} = \pm 5\lambda_{\rm SO}$, $\varepsilon^{\rm R}_{{\rm K}'\downarrow} = \pm 7\lambda_{\rm SO}$ for the right region. It can be seen that K valley is spin-polarized and K′ valley is spin-degenerated in the left region while the contrary is the case in the right region, as shown in Fig. 2(a), which depicts the band structures of the three regions. The length of the central region is set as $d = 0.8\xi$, where $\xi = 3at/2\Delta$ is the superconducting coherence length. In addition, the chemical potentials of the two regions are set as $U_{\rm L} = -\lambda_{\rm SO}$ and $U_{\rm R} = \lambda_{\rm SO}$. Hence, the Fermi surface is just at the bottom of the conduction band of the left region and at the top of the valence band of the right region. In this case, we calculate the conductances $g_{\rm AR}$, $g_{\rm CAR}$ and $g_{\rm EC}$ *versus* the incident energy E, which are shown in Fig. 2(b) with different lines. It is worth noting that all of the conductance values in our paper are normalized by the ballistic normal conductance $g_0 = 2e^2N(E)/h$, where $N(E) = EW/(\pi\hbar v_{\rm F})$ represents the number of the transverse modes. From Fig. 2(b), we can see that $g_{\rm CAR}$ is much more than $g_{\rm AR}$ and $g_{\rm EC}$, *i.e.*, $g_{\rm CAR}$ dominates while $g_{\rm AR}$ and $g_{\rm EC}$ are both suppressed. This means the pure crossed Andreev reflection can be generated in our system by the control of the electric field and the light field. The emergence of such a phenomenon can be explained well by Fig. 2(a). The incident

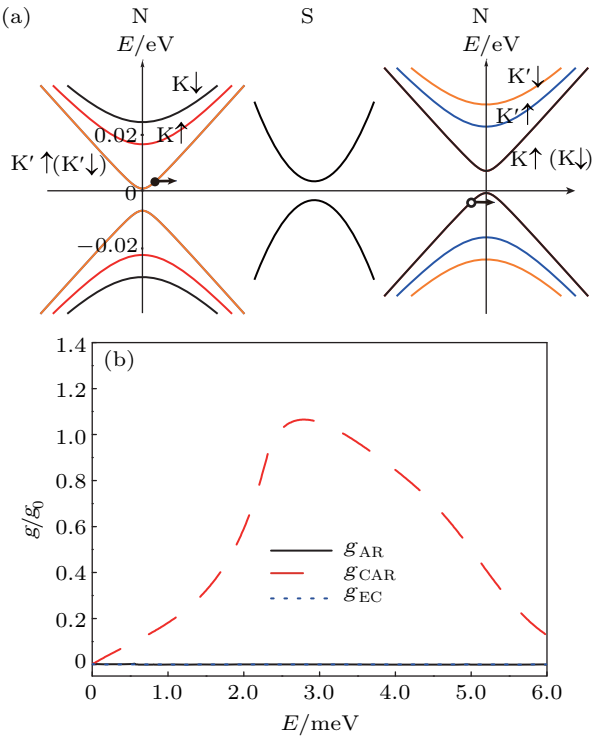


Fig. 2. (color online) (a) The energy spectra of the three regions. (b) The conductances $g_{\rm AR}$ (solid line), $g_{\rm CAR}$ (dash line), and $g_{\rm EC}$ (dotted line) *versus* the incident energy E for the antiparallel electric fields $elE^{\rm L}_z = -elE^{\rm R}_z = \lambda$. The other parameters are set as the light field strength $\lambda = 3\lambda_{\rm SO}$, the superconducting region length $d = 0.8\xi$, the chemical potentials of the two normal regions $-U_{\rm L} = U_{\rm R} = \lambda_{\rm SO}$ and the superconducting pairing potential $\Delta = 2$ meV.

energy of Fig. 2(b) is under 6.0 meV, so the incident electron from the left region locates at K′ valley. At the same time, the right region provides an electron from K valley. The two electrons from different valleys can constitute a cooper pair, which produces the CAR conductance $g_{\rm CAR}$. Moreover, because there is no K valley channels existing under 6 meV in the left region, the AR conductance $g_{\rm AR}$ is almost 0. Similarly, the EC conductance $g_{\rm EC}$ is suppressed, because there is no K′ valley channels existing under 6 meV in the right region. Hence, the pure CAR conductance can be obtained without the accompanying of the AR and EC conductances in our system.

Whereafter, we discuss the influence of the superconducting region length d and the light field strength λ on the CAR conductance in Fig. 3. Thereinto, the electric field strengths are set as $elE_z^{\rm L} = -elE_z^{\rm R} = \lambda$ and the chemical potentials are set as $U_{\rm L} = -\lambda_{\rm SO}$, $U_{\rm R} = \lambda_{\rm SO}$. Figure 3(a) shows $g_{\rm CAR}$ *versus* E for different d with λ fixed at $3\lambda_{\rm SO}$. It can be found that the difference of d will affect $g_{\rm CAR}$ greatly. There are different peak values for different lines. For the line of $d = 0.5\xi$, the peak value appears at about $E = 1.0$ meV, while for the line of $d = \xi$, the peak value appears at about $E = 2.0$ meV. In addition, when $d = 2\xi$, which exceeds ξ much, the value of $g_{\rm CAR}$ is much smaller than ones of the other three lines. This result is corresponding to Fig. 3(b), where we calculate $g_{\rm CAR}$ as a function of d for different E. It is obvious to see that the nonlocal conductance exhibits an oscillatory behavior with d because of the quasiparticle interference in the superconducting gap. There appear the conductance peaks whenever the subgap superconducting quasiparticle wave vector matches the resonance wave vector $k_x = n\pi/d$. Moreover, for $E = 1.0$ meV and 2.0 meV, the biggest peak appears respectively around $d = 0.5\xi$ and 1.0ξ, and $g_{\rm CAR}$ decays rapidly when d exceeds the superconducting coherence length, which is identical with the result in Fig. 3(a).

In the same way, the nonlocal conductance *versus* the incident energy for different light field strengths is described in Fig. 3(c). It can be seen that $g_{\rm CAR}$ for $\lambda = 0.5\lambda_{\rm SO}$ is much smaller than ones for $\lambda = 2\lambda_{\rm SO}$ and $3\lambda_{\rm SO}$. It is due to that when $\lambda = 0.5\lambda_{\rm SO}$, $g_{\rm AR}$ and $g_{\rm EC}$ are no longer suppressed, and then $g_{\rm CAR}$ is reduced. Meanwhile, we also find the difference between the two lines of $\lambda = 2\lambda_{\rm SO}$ and $3\lambda_{\rm SO}$ is very small because the band structures in the two cases are very similar. Figure 3(d) depicts the nonlocal conductance as a function of the light field strength for different incident energies. When λ increases gradually, $g_{\rm CAR}$ first has an obvious change and then almost keeps unchanged, which is consistent with Fig. 3(c).

3.2. The switch effects

3.2.1. Pure EC conductance

Now, we keep the parameters of the left region the same as Fig. 2 and change the parameters of the right region as $elE_z^{\rm R} = \lambda = 3\lambda_{\rm SO}$. Thus, the two normal regions have the identical band structures, as shown in Fig. 4(a), where the chemical potentials are set as $U_{\rm L} = U_{\rm R} = -\lambda_{\rm SO}$. In this situation, when the incident energy is under the bottom of the K ↑ band ($\sim 4\lambda_{\rm SO}$), an electron of K′ valley from the left region can tunnel into the right region to generate the EC conductance $g_{\rm EC}$. However, the CAR conductance $g_{\rm CAR}$ and the AR conductance $g_{\rm AR}$ are both almost zero because there are no channels of K valley for the CAR and AR processes in the two normal regions. As a result, a pure $g_{\rm EC}$ with $g_{\rm CAR}$ and $g_{\rm AR}$ being zero can be produced, as depicted in Fig. 4(b). Combined with Fig. 2(b), we find a switch effect between the nonlocal transports, *i.e.*, the perfect CAR and the perfect EC processes,

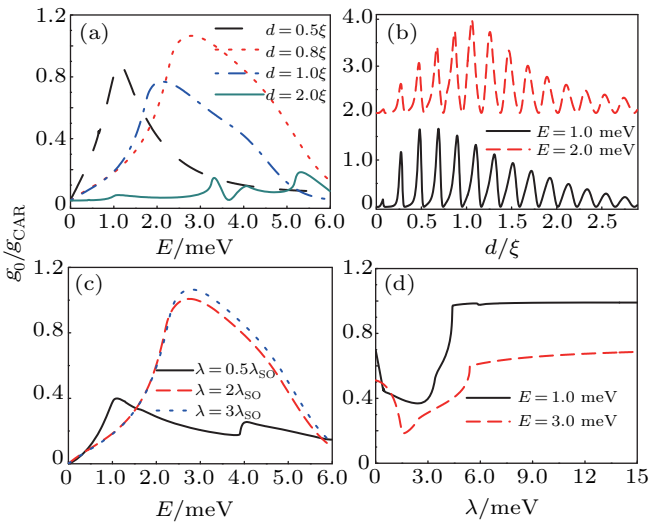


Fig. 3. (color online) The parameter dependence of the CAR conductance. (a) $g_{\rm CAR}$ *versus* E for different d and (b) $g_{\rm CAR}$ *versus* d for different E with $elE_z^{\rm L} = -elE_z^{\rm R} = \lambda = 3\lambda_{\rm SO}$. (c) $g_{\rm CAR}$ *versus* E for different λ and (d) $g_{\rm CAR}$ *versus* λ for different E with $d = 0.8\xi$ and $elE_z^{\rm L} = -elE_z^{\rm R} = \lambda$. The chemical potentials are still set as $-U_{\rm L} = U_{\rm R} = \lambda_{\rm SO}$.

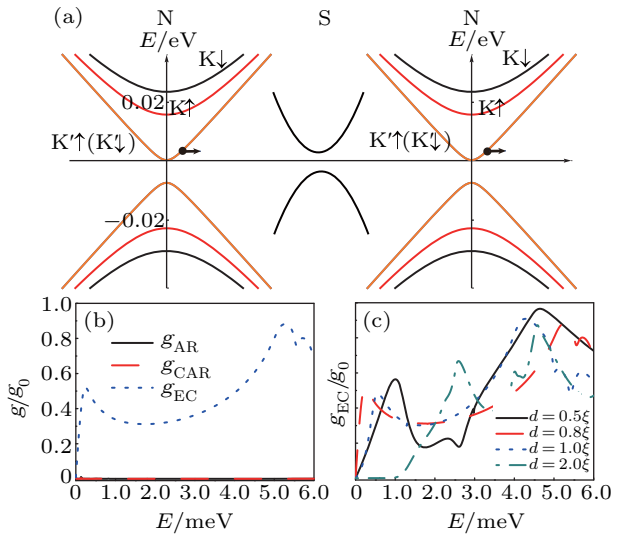


Fig. 4. (color online) (a) The band structures of the three regions. (b) $g_{\rm AR}$, $g_{\rm CAR}$, and $g_{\rm EC}$ *versus* E with $d = 0.8\xi$. (c) $g_{\rm EC}$ *versus* E for different d. Here, the parallel electric fields $elE_z^{\rm L} = elE_z^{\rm R} = \lambda$ are applied to the two normal regions, the light field strength is set as $\lambda = 3\lambda_{\rm SO}$ and the chemical potentials are chosen as $U_{\rm L} = U_{\rm R} = -\lambda_{\rm SO}$.

by reversing the perpendicular electric field of the right region from $elE_z^{\mathrm{R}} = -\lambda$ to $elE_z^{\mathrm{R}} = \lambda$. In other words, transmission particles from the right region can change from holes (CAR) to electrons (EC) just by flipping the direction of the electric field. Besides, the EC conductance spectra for different superconducting region length d are illustrated in Fig. 4(c). As seen, g_{EC} varies with E non-monotonically and has different variation trends for different d.

3.2.2. Pure AR conductance

In this section, we set the parameters as $\lambda = \lambda_{\mathrm{SO}}$, $elE_z^{\mathrm{L}} = -\lambda$, $elE_z^{\mathrm{R}} = 7\lambda$, and $d = 0.8\xi$. The band structures of the normal regions, calculated by Eq. (7), are shown in Fig. 5(a), where the bands of K $\uparrow$, K $\downarrow$, and K$'$ $\uparrow$ are degenerated in the left region and the bands of K $\uparrow$ and K$'$ $\uparrow$ are degenerated in the right region. Simultaneously, utilizing Eq. (8), we can obtain the values on the K and K$'$ points of the bands: $\varepsilon^{\mathrm{L}}_{\mathrm{K}\uparrow} = \varepsilon^{\mathrm{L}}_{\mathrm{K}\downarrow} = \varepsilon^{\mathrm{L}}_{\mathrm{K}'\uparrow} = \pm\lambda_{\mathrm{SO}}$ and $\varepsilon^{\mathrm{L}}_{\mathrm{K}'\downarrow} = \pm 3\lambda_{\mathrm{SO}}$ for the left normal region, and $\varepsilon^{\mathrm{R}}_{\mathrm{K}'\downarrow} = \pm 5\lambda_{\mathrm{SO}}$, $\varepsilon^{\mathrm{R}}_{\mathrm{K}\uparrow} = \varepsilon^{\mathrm{R}}_{\mathrm{K}'\uparrow} = \pm 7\lambda_{\mathrm{SO}}$ and $\varepsilon^{\mathrm{R}}_{\mathrm{K}\downarrow} = \pm 9\lambda_{\mathrm{SO}}$ for the right normal region, by which the gaps of all the bands can be obtained. The chemical potentials are set as $U_{\mathrm{L}} = -\lambda_{\mathrm{SO}}$ and $U_{\mathrm{R}} = 0$, ensuring the Fermi surface at the bottom of the conduction band of the left region. When the incident energy is low ($E < 2\lambda_{\mathrm{SO}}$), the three kinds of conductances g_{CAR}, g_{AR} and g_{EC} would be suppressed due to the fact that there are neither channels for CAR or EC processes in the right region nor channels for AR process in the left region.

However, the situation changes when the incident energy exceeds $2\lambda_{\mathrm{SO}}$. As seen in Fig. 5(b), the conductances g_{CAR} and g_{EC} are still suppressed, but g_{AR} has evident values. The reason is that there are yet no transport channels for CAR or EC processes existing owing to the gap about $10\lambda_{\mathrm{SO}}$ in the right region, while for incident energies above $2\lambda_{\mathrm{SO}}$, there exist the hole bands in the left region making the Andreev reflection happen. More specifically, when an electron above $2\lambda_{\mathrm{SO}}$ enters into the superconductor from the left region, a corresponding hole is reflected from the left region at the same time, which produces the AR conductance. That means the pure AR conductance also can be acquired in the present case. In addition, figure 5(c) shows the local conductance g_{AR} *versus* the incident energy E for different superconducting region length d. It is observed that the lines of g_{AR} are not monotonous and have different variation trends with E for different d. For $d = 0.5\xi$, g_{AR} has bigger values when E is lower, while for $d = 0.8\xi$, g_{AR} has bigger values when E is higher. Therefore, not only pure CAR and pure EC but also pure AR can be obtained by controlling the light and electric field. In other words, our system can realize a switch effect among the exclusive CAR, the exclusive EC and the exclusive AR.

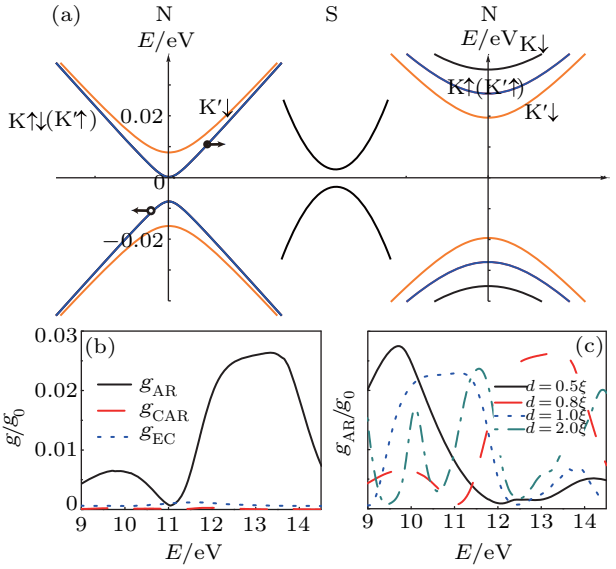


Fig. 5. (color online) (a) The band structures of the three regions. (b) g_{AR}, g_{CAR}, and g_{EC} *versus* E with $d = 0.8\xi$. (c) g_{AR} *versus* E for different d. Therein, the antiparallel electric fields $elE_z^{\mathrm{L}} = -\lambda$ and $elE_z^{\mathrm{R}} = 7\lambda$ are respectively applied to the left and right regions, the light field strength is set as $\lambda = \lambda_{\mathrm{SO}}$ and the chemical potentials are chosen as $U_{\mathrm{L}} = -\lambda_{\mathrm{SO}}$ and $U_{\mathrm{R}} = 0$.

4. Summary

In conclusion, we have investigated the quantum transport properties in a monolayer silicene-based N/S/N junction. The off-resonant circularly polarized light field and the perpendicular electric field are applied to the two terminals simultaneously. Due to different spin and valley polarizations of the band structures in the two normal regions, we can obtain the exclusive CAR process without the EC and AR processes. Also, the exclusive EC and AR processes can be respectively acquired by the change of the bands under the coaction of the light and electric fields. Hence, not only the switch between the nonlocal transports (the CAR and EC processes) but also the switch among the two nonlocal transports and the local transport (the AR process) can be realized in our system. These results will potentially provide some intriguing insights into the correlation transport in silicene-based hybrid structures.

References

[1] Oughaddou H, Enriquez H, Tchalala M R, Yildirim H, Mayne A J, Bendounan A, Dujardin G, Ait Ali M and Kara A 2015 *Prog. Surf. Sci.* **90** 46
[2] Zhao J, Liu H, Yu Z, Quhe R, Zhou S, Wang Y, Li C C, Zhong H, Han N, Lu J, Yao Y and Wu K 2016 *Prog. Mater. Sci.* **83** 24
[3] Guzmán-Verri G G and Lew Yan Voon L C 2007 *Phys. Rev. B* **76** 075131
[4] Cahangirov S, Topsakal M, Aktürk E, Sahin H and Ciraci S 2009 *Phys. Rev. Lett.* **102** 236804
[5] Drummond N D, Zólyomi V and Fal'ko V I 2012 *Phys. Rev. B* **85** 075423
[6] Ni Z, Liu Q, Tang K, Zheng J, Zhou J, Qin R, Gao Z, Yu D and Lu J 2012 *Nano Lett.* **12** 113
[7] Chen L, Liu C C, Feng B, He X, Cheng P, Ding Z, Meng S, Yao Y and Wu K 2012 *Phys. Rev. Lett.* **109** 056804

[8] Liu C C, Jiang H and Yao Y 2011 *Phys. Rev. B* **84** 195430
[9] Ezawa M 2013 *Phys. Rev. Lett.* **110** 026603
[10] Lalmi B, Oughaddou H, Enriquez H, Kara A, Vizzini S, Ealet B and Aufray B 2010 *Appl. Phys. Lett.* **97** 223109
[11] Vogt P, De Padova P, Quaresima C, Avila J, Frantzeskakis E, Asensio M C, Resta A, Ealet B and Le Lay G 2012 *Phys. Rev. Lett.* **108** 155501
[12] Johnson N, Vogt P, Resta A, Padova P D, Pere I, Muir D, Kurmaev E Z, Lay G L and Moewes A 2014 *Adv. Funct. Mater.* **24** 5253
[13] Fleurence A, Friedlein R, Ozaki T, Kawai H, Wang Y and Yamada-Takamura Y 2012 *Phys. Rev. Lett.* **108** 245501
[14] Meng L, Wang Y, Zhang L, Du S, Wu R, Li L, Zhang Y, Li G, Zhou H, Hofer W A and Gao H J 2013 *Nano Lett.* **13** 685
[15] Chiappe D, Scalise E, Cinquanta E, Grazianetti C, Broek B, Fanciulli M, Houssa M and Molle A 2014 *Adv. Mater.* **26** 2096
[16] Tao L, Cinquanta E, Chiappe D, Grazianetti C, Fanciulli M, Dubey M, Molle A and Akinwande D 2015 *Nat. Nanotechnol.* **10** 227
[17] Linder J and Yokoyama T 2014 *Phys. Rev. B* **89** 020504
[18] Li H 2016 *Phys. Rev. B* **94** 075428
[19] Li H, Wang R and Ting C S 2016 *Phys. Rev. B* **94** 085422
[20] Zhou X and Jin G 2016 *Phys. Rev. B* **94** 165436
[21] Paul G C and Saha A 2017 *Phys. Rev. B* **95** 045420
[22] Vosoughinia S, Hajati Y and Rashedi G 2017 *J. Appl. Phys.* **122** 043906
[23] Soodchomshom B, Niyomsoot K and Pattrawutthiwong E 2018 *Physica E* **97** 375
[24] Amico L, Fazio R, Osterloh A and Vedral V 2008 *Rev. Mod. Phys.* **80** 517
[25] Horodecki R, Horodecki P, Horodecki M and Horodecki K 2009 *Rev. Mod. Phys.* **81** 865
[26] Brunner N, Cavalcanti D, Pironio S, Scarani V and Wehner S 2014 *Rev. Mod. Phys.* **86** 419
[27] Caruso F, Giovannetti V, Lupo C and Mancini S 2014 *Rev. Mod. Phys.* **86** 1203
[28] Recher P, Sukhorukov E V and Loss D 2001 *Phys. Rev. B* **63** 165314
[29] Chtchelkatchev N M, Blatter G, Lesovik G B and Martin T 2002 *Phys. Rev. B* **66** 161320
[30] Byers J M and Flatté M E 1995 *Phys. Rev. Lett.* **74** 306
[31] Deutscher G and Feinberg D 2000 *Appl. Phys. Lett.* **76** 487
[32] Buzdin A I 2005 *Rev. Mod. Phys.* **77** 935
[33] Hofstetter L, Csonka S, Nygård J and Schönenberger C 2009 *Nature* **461** 960
[34] Schindele J, Baumgartne A and Schönenberger C 2012 *Phys. Rev. Lett.* **109** 157002
[35] Schroer A, Silvestrov P G and Recher P 2015 *Phys. Rev. B* **92** 241404(R)
[36] Mélin R and Feinberg D 2004 *Phys. Rev. B* **70** 174509
[37] Herrmann L G, Portier F, Roche P, Yeyati A L, Kontos T and Strunk C 2010 *Phys. Rev. Lett.* **104** 026801
[38] Wei J and Chandrasekhar V 2010 *Nat. Phys.* **6** 494
[39] Cayssol J 2008 *Phys. Rev. Lett.* **100** 147001
[40] Veldhorst M and Brinkman A 2010 *Phys. Rev. Lett.* **105** 107002
[41] Linder J, Zareyan M and Sudbø A 2009 *Phys. Rev. B* **80** 014513
[42] Majidi L and Asgari R 2014 *Phys. Rev. B* **90** 165440
[43] Chen W, Shen R, Sheng L, Wang B G and Xing D Y 2011 *Phys. Rev. B* **84** 115420
[44] Reinthaler R W, Recher P and Hankiewicz E M 2013 *Phys. Rev. Lett.* **110** 226802
[45] Zhang Y T, Hou Z, Xie X C and Sun Q F 2017 *Phys. Rev. B* **95** 245433
[46] Qi F, Cao J and Jin G 2018 *Phys. Rev. B* **98** 045422
[47] Kitagawa T, Oka T, Brataas A, Fu L and Demler E 2011 *Phys. Rev. B* **84** 235108
[48] Zhou X, Xu Y and Jin G 2015 *Phys. Rev. B* **92** 235436
[49] Liu C C, Jiang H and Yao Y 2011 *Phys. Rev. B* **84** 195430
[50] Lee D H and Joannopoulos J D 1981 *Phys. Rev. B* **23** 4997
[51] López Sancho M P, López Sancho J M and Rubio J 1984 *J. Phys. F: Met. Phys.* **14** 1205